



TITLE:

ISRM Suggested Method for Laboratory Acoustic Emission Monitoring

AUTHOR(S):

Ishida, Tsuyoshi; Labuz, Joseph F.; Manthei, Gerd; Meredith, Philip G.; Nasser, M. H. B.; Shin, Koichi; Yokoyama, Tatsuya; Zang, Arno

CITATION:

Ishida, Tsuyoshi ...[et al]. ISRM Suggested Method for Laboratory Acoustic Emission Monitoring. Rock Mechanics and Rock Engineering 2017, 50(3): 665-674

ISSUE DATE:

2017-03-01

URL:

<http://hdl.handle.net/2433/219136>

RIGHT:

The final publication is available at Springer via <http://dx.doi.org/10.1007/s00603-016-1165-z>; The full-text file will be made open to the public on 01 March 2018 in accordance with publisher's 'Terms and Conditions for Self-Archiving'; This is not the published version. Please cite only the published version.; この論文は出版社版ではありません。引用の際には出版社版をご確認ください。

ISRM Suggested Method

for Laboratory Acoustic Emission Monitoring

Tsuyoshi ISHIDA^{1,*}, Joseph F. Labuz², Gerd Manthei³, Philip G. Meredith⁴,
M.H.B. Nasser⁵, Koichi Shin⁶, Tatsuya Yokoyama⁷, Arno Zang⁸

¹Dept. of Civil and Earth Resources Engineering, Kyoto University, C-Cluster, Katsura Campus of
Kyoto University, Nishikyo-ku, Kyoto, 615-8540 JAPAN

²Department of Civil, Environmental, and Geo- Engineering, University of Minnesota,
Minneapolis USA

³THM University of Applied Sciences, Wiesenstraße 14, 35390 Gießen, Germany

⁴Department of Earth Sciences, University College London, Gower Street, London WC1E 6BT, UK

⁵Department of Civil Engineering, University of Toronto, 35 St. George Street, Toronto, Ontario, M5S
1A4, Canada

⁶Central Research Institute of Electric Power Industry, 1646 Abiko, Abiko-city, Chiba-prefecture, 270-
1194 Japan

⁷Energy Business Division, OYO Corporation, 2-2-19 Daitakubo, Minami-ku, Saitama, 336-0015,
Japan

⁸Section 2.6, Seismic Hazard and Stress Field, Helmholtz-Zentrum Potsdam, German Research Center
for Geosciences-GFZ, Telegrafenberg, 14473 Potsdam, Germany

Please send all written comments on these ISRM Suggested Methods to Prof. R. Ulusay, President of the ISRM Commission
on Testing Methods, Hacettepe University, Geological Engineering Department, 06800 Beytepe, Ankara, Turkey at
resat@hacettepe.edu.tr.

* T. Ishida (corresponding author) e-mail: ishida.tsuyoshi.2a@kyoto-u.ac.jp

1. Introduction

Acoustic emission (AE) is defined as high frequency elastic waves emitted from defects
such as small cracks (microcracks) within a material when stressed, typically in the
laboratory. AE is a similar phenomenon to microseismicity (MS), as MS is induced by
fracture of rock at an engineering scale (*e.g.* rockbursts in mines), that is, in the field. Thus,
seismic monitoring can be applied to a wide variety of rock engineering problems, and AE is
a powerful method to investigate processes of rock fracture by detecting microcracks prior

to macroscopic failure and by tracking crack propagation.

A basic approach involves the use of a single channel of data acquisition, such as with a digital oscilloscope, and analyzing the number and rate of AE events. Perhaps the most valuable information from AE is the source location, which requires recording the waveform at several sensors and determining arrival times at each. Thus, investing in a multichannel data acquisition system provides the means to monitor dynamics of the fracturing process.

The purpose of this suggested method is to describe the experimental setup and devices used to monitor AE in laboratory testing of rock. The instrumentation includes the AE sensor, pre-amplifier, frequency (noise) filter, main amplifier, AE rate counter, and A/D (analog-to-digital) recorder, to provide fundamental knowledge on material and specimen behavior in laboratory experiments. When considering in-situ seismic monitoring, the reader is referred to the relevant ISRM Suggested Method specifically addressing that topic (Xiao et al., 2016).

2. Brief Historical Review

2.1 Early Studies of AE Monitoring for Laboratory Testing

AE / MS monitoring of rock is generally credited to Obert and Duval (1945) in their seminal work related to predicting rock failure in underground mines. Laboratory testing was later used to understand better the failure process of rock (Mogi 1962a). For example, the nature of crustal-scale earthquakes from observations of micro-scale fracture phenomena was a popular topic. Mogi (1968) discussed the process of foreshocks, main shocks, and aftershocks from AE activity monitored through failure of rock specimens. Scholz (1968b, 1968c) studied the fracturing process of rock and discussed the relation between microcracking and inelastic deformation. Nishizawa et al. (1984) examined focal mechanisms of microseismicity, and Kusunose and Nishizawa (1986) discussed the concept of the seismic gap from AE data obtained in their laboratory experiments. Spetzler et al. (1991) discussed stick slip events in pre-fractured rock with various surface roughness by combining acoustic emission with holographic interferometry measurements. Compiling years of study, Scholz (2002) and Mogi (2006) published books on rock failure processes from a geophysics perspective. Hardy (1994, 2003) focused on geoengineering applications of AE, while Grosse and Ohtsu (2008) edited topics on the use of AE as a health monitoring method for civil engineering structures.

2.2 AE Monitoring in Novel Application

Many researchers have used AE in novel ways. Yanagidani et al. (1985) performed creep experiments under constant uniaxial stress and used AE location data to elucidate a cluster of microcracks prior to macro-scale faulting. His research group also developed the concept

of using AE rate to control compression experiments (Terada et al. 1984). Using this method, Lockner et al. (1991) conducted laboratory experiments under controlled loading by keeping the AE rate constant and discussed the relation between fault growth and shear fracture by imaging AE nucleation and propagation.

Besides the research on rock fracturing, AE monitoring has been applied to stress measurement using the Kaiser effect (Kaiser, 1953), that is the stress memory effect with respect to AE occurrence in rock. This application was started by Kanagawa et al. (1976) and patented by Kanagawa and Nakasa (1978). Lavrov (2003) presented a historical review of the approach.

2.3 AE Monitoring with Development of Digital Technology

With development of digital technology, AE instrumentation advanced through the use of high speed and large capacity data acquisition systems. For example, using non-standard asymmetric compression specimens, Zang et al. (1998, 2000) located AE sources, analyzed the fracturing mechanism, and compared the results with images of X-ray CT scans. Studies of the fracture process zone include Zietlow and Labuz (1998), Zang et al. (2000), and Nasser et al. (2006), among others. Benson et al. (2008) conducted a laboratory experiment to simulate volcano seismicity and observed low frequency AE events exhibiting a weak component of shear (double-couple) slip, consistent with fluid-driven events occurring beneath active volcanoes. Heap et al. (2009) conducted stress-stepping creep tests under pore fluid pressure and discussed effects of stress corrosion using located AE data. Chen and Labuz (2006) performed indentation tests of rock using wedge-shaped tools and compared the damage zone shown with located AE sources to theoretical predictions.

Ishida et al. (2004, 2012) conducted hydraulic fracturing laboratory experiments using various fluids, including supercritical carbon dioxide, and discussed differences in induced cracks due to fluid viscosity using distributions of AE sources and fault plane solutions. Using AE data from triaxial experiments, Goebel et al. (2012) studied stick-slip sequences to get insight into fault processes, and Yoshimitsu et al. (2014) suggested that both millimeter scale fractures and natural earthquakes of kilometer scale are highly similar as physical processes. The similarity is also supported by Kwiatak et al. (2011) and Goodfellow and Young (2014).

Moment tensor analysis of AE events has been applied to laboratory experiments. Shah and Labuz (1995) and Sellers et al. (2003) analyzed source mechanisms of AE events under uniaxial loading, while Graham et al. (2010) and Manthei (2005) analyzed them under triaxial loading. Kao et al. (2011) explained the predominance of shear microcracking in mode I fracture tests through a moment tensor representation of AE as displacement discontinuities.

3. Devices for AE Monitoring

One of the simplest loading arrangements for AE monitoring in the laboratory is that for uniaxial compression of a rock specimen; Figure 1 shows a typical arrangement. Since an AE signal detected at a sensor is of very low amplitude, the signal is amplified through a pre-amplifier and possibly a main amplifier. Typically the signal travels through a coaxial cable (a conductor with a wire-mesh to shield the signal from electromagnetically induced noise) with a BNC (Bayonet Neill Conelman) connector. It is usually necessary to further eliminate noise, so a band pass filter, a device that passes frequencies within a certain range, is used. In the most basic setup using one sensor only, the rate of AE events is counted by processing the detected signals. In more advanced monitoring, for example, for source location of AE events, more sensors are used and AE waveforms detected at the respective sensors are recorded through an A/D converter. Figure 2a shows a twelve sensor array for a core 50 mm in diameter and 100 mm in length (Zang et al. 2000); an AE-rate controlled experiment was performed to map a fracture tip by AE locations, as shown in Figure 2b. To locate AE, it is advantageous for the sensors to be mounted so as to surround the source, as shown in Figure 2. The three lines indicate paths to monitor P-waves transmitted from sensor No. 12 by using it as an emitter.

3.1 AE Sensor

AE sensors are typically ceramic piezoelectric elements. The absolute sensitivity is defined as the ratio of an output electric voltage to velocity or pressure applied to a sensitive surface of a sensor in units, V/(m/s) or V/kPa, and its order is 0.1 mV/kPa. However, the absolute sensitivity often depends on the calibration method (McLaskey and Glaser 2012). From this reason, a sensitivity of an AE sensor is usually stated as relative sensitivity in units of dB.

Figure 3 shows a typical sensor with a pre-amplifier. AE sensors can be classified into two types, depending on frequency characteristics: resonance and broadband. Figure 4a illustrates the frequency response of a resonance type sensor, while Figure 4b shows the characteristics of a broadband type sensor. Both sensors have a cylindrical shape with the same size of 18 mm in diameter and 17 mm in height. However, it can be seen that the resonance type sensor (Figure 4 (a)) has a clear peak around 150 kHz while the broadband type (Figure 4(b)) has a response without any clear peak from 200 to 800 kHz. Since the resonance type detects an AE event at the most sensitive frequency, it tends to produce a signal having large amplitude in a frequency band close to its resonance frequency, independent of a dominant frequency of the actual AE waveform. As a result, the resonance type sensor conceals the characteristic frequency of the “actual” AE signal and it may lose

important information about the source.

On the other hand, it is often claimed that the broadband type records a signal corresponding to the original waveform. However, comparing Figure 4a and 4b illustrates that the sensitivity of the broadband type is on average 10 dB less than that of the resonance type. For this reason, the resonance type sensor is often employed for AE monitoring. In an early study on rock fracturing (Zang et al. 1996), both sensor types, resonance and broadband, were used to investigate fracture mechanisms in dry and wet sandstone. Further, broadband sensors have been developed to provide high fidelity signals for source characterization (Proctor 1982; Boler et al. 1984; Glaser et al. 1998; McLaskey and Glaser 2012; McLaskey et al. 2014). One additional item that should be noted is that sensor selection should be dependent on rock type. For weak rock like mudstone having low stiffness and high attenuation, an AE sensor having a lower resonance frequency is recommended because it is difficult to monitor high frequency signals in a weak rock.

For counting AE events, two or more sensors should be used to check the effect of sensor position and distinguish AE signals from noise. For 3D source locations of AE events, at least five sensors (or four sensors and one other piece of information) are necessary, because of the four unknowns (source coordinates x , y , z , and an occurrence time t) and the quadratic nature of the distance equation. More than eight sensors are usually used to improve the locations of the AE events through an optimization scheme (Salamon and Wiebols 1974).

For setting an AE sensor on a cylindrical specimen, it is recommended to machine a small area of the curved surface to match the planar end of the sensor. To adhere the sensor on the specimen, various kinds of adhesives can be used, such as a cyanoacrylate-based glue or even wax, which allows easy removal. It is recommended to use a consistent but small amount of adhesive so as to reduce the coupling effect (Shah and Labuz 1995). Many AE sensors are designed to operate within a pressure vessel, so from the perspective of the AE technique, the issues are the same for uniaxial and triaxial testing.

3.2 Amplifiers and Filters

When AE events generated in a specimen are detected by an AE sensor, the motion induces an electric charge on the piezoelectric element. A pre-amplifier connected to the AE sensor transfers the accumulated electric charge as a voltage signal with a gain setting from 10 to 1000 times. Thus, a pre-amplifier should be located within close proximity (less than one meter) from an AE sensor, and some commercial AE sensors are equipped with integrated pre-amplifiers. Since a pre-amplifier needs a power supply to amplify a signal, it should be connected to a “clean” power unit so that the signal is not buried in noise.

A signal amplified by a pre-amplifier is often connected to another amplifier, and a

frequency filter is inserted to reduce noise. A high pass filter passes only a signal having frequencies higher than a set frequency to eliminate the lower frequency noises; a low pass filter eliminates the higher frequency noise. A filter that combines the two is called a band pass filter and is often used as well. When the AE sensor shown in Figure 3, having a resonance frequency of 150 kHz is employed, a band pass filter from 20 to 2000 kHz is common. A band frequency of the filter should be selected depending on frequency of the anticipated waves and on the frequency of the noise.

3.3 AE Count and Rate

The AE count means a number of AE occurrence, whereas the AE count rate means the AE count per a certain time interval. Figure 5 shows a typical example of AE count rates monitored in a uniaxial compression test on a rock core. It is possible to show a relation between impending failure and AE occurrence, when AE count rates are shown with a load-displacement curve. Noting that the AE count rate on the y-axis is plotted on a logarithmic scale, a burst of AE is observed just before failure (peak axial stress) of the specimen. This suggests that AE count rate is a sensitive parameter for observing failure.

Methods to determine AE counts are classified into ring-down count and event count. In both cases, a certain voltage level called the threshold or discriminate level is set for AE recording (Figure 6). The level is set slightly higher than the background noise level regardless of rock properties and test conditions, and consequently the AE count and rate depend on the threshold level. In a ring-down counting method, a TTL (Transistor-Transistor-Logic) signal is produced every time a signal exceeds a threshold level. In the case shown in Figure 6b, five TTL signals are produced for one AE event, and they are sent to a counter as five counts. On the other hand, an event count records one count for each AE event; a typical method generates a low frequency signal that envelopes the original signal (Figure 6c). After that, when the low frequency signal exceeds a threshold level, one TTL signal is produced and sent to a counter. The function to generate the TTL signals should be mounted in a main amplifier or a rate counter as shown in Figure 1.

Whichever method is selected, AE counts and rates depend on the gain of the amplifiers and the threshold level. Thus, the threshold level should be reported together with the respective gains of the pre-amplifier and amplifier, along with the method selected for counting. Nonetheless, comparison of AE counts and rates between two experiments should be done cautiously, as the failure mechanism, or more importantly, coupling may differ. Sensitivity of an AE sensor is strongly affected by the coupling condition between the sensor and specimen. For example, the area and shape of the couplant (adhesive) can be different, even if the couplant is applied in the same manner (Shah and Labuz 1995). For these reasons, comparison of exact numbers of AE counts and rates between two

experiments is not recommended, although their changes within an experiment become very good indices for identifying the accumulation of damage and extension of fracture.

3.4 Recording AE Waveforms

AE waveforms contain valuable information on the fracture process, including location of the AE source. AE waveforms can be recorded by an A/D converter and stored in memory.

(1) Principle of A/D conversion

To record an AE waveform, as shown in Figure 7, an electric signal from an AE sensor flows through an A/D converter. When the amplitude of the signal exceeds a threshold level, which is set in advance, a certain “length” of the signal before and after the threshold is stored in memory. While the voltage level set in advance is called the threshold level or discriminate level, the time when a signal voltage exceeds the level is called the trigger time or trigger point. Note that “trigger” can mean either to start a circuit or to change the state of a circuit by a pulse, while, in some cases, “trigger” means the pulse itself. In actual monitoring, the TTL signal for the AE rate counter is usually branched and connected into an A/D converter as the trigger signal. Sometimes, to avoid recording waveforms that cannot provide sufficient information to determine a source location, a logic of AND/OR for triggering is used; e.g. triggering occurs only when signals of two sensors set in the opposite position on the specimen exceed a threshold level at the same time. Indeed, it is possible to use much more complex logic. Using an arrival time picking algorithm, automatic source location of AE events can be realized.

When recording an AE waveform, a time period before the trigger time needs to be specified and this time period is called the pre-trigger or delay time. In A/D conversion, voltages of an analog signal are read with a certain time interval and the voltages are stored in memory as digital numbers. The principle is illustrated in an enlarged view of an initial motion of the waveform in the lower part of Figure 7. The time interval, Δt , is called the sampling time. On the other hand, the recording time of a waveform is sometimes designated as a memory length of an A/D converter.

For example, in an hydraulic fracturing experiment on a 190 mm cubic granite specimen (Ishida et al. 2004) and a uniaxial loading experiment on a 300 x 200 x 60 mm rectangular tuff specimen (Nakayama et al. 1993), the researchers used a sensor having a resonance frequency of 150 kHz, which is shown in Figure 3, and monitored AE signals by using a sampling time of 0.2 μ s and a memory length of 2 k (2,048 words). In this case, the recording time period was around 0.4 ms (0.2 μ s x 2,048). The pre-trigger was set at 1 k, one-half of the recording time; the pre-trigger is often reported as memory length rather than in real time.

(2) Sampling Time

To explain selection of a proper sampling time, consider the case where a sine curve is converted at only four points from analog data to digital. If the sampling points meet the maximum and the minimum points of the curve, as shown in Figure 8a, a signal reproduced by linear interpolation from the converted digital data is similar to the original signal. However, if the sampling points are moved 1/8 cycle along the time axis, as shown in Figure 8b, the reproduced signal is much distorted from the original one. These two examples suggest that four sampling points for a cycle are not sufficient and at least ten points for a cycle are needed to reproduce the waveform correctly from the converted digital data.

A specification of an A/D converter usually shows a reciprocal number of the minimum sampling time. For example, if the minimum sampling time is 1 μ s, the specification shows the reciprocal number, 1 MHz, as the maximum monitoring frequency. However, this does not mean the frequency of a waveform that can be correctly reproduced. In this case, around one-tenth of the frequency, or 100 kHz, can be recorded.

(3) Resolution of Amplitude

Whereas the sampling time corresponds to the resolution along the x-axis of an A/D converter, the resolution capability along the y-axis (amplitude), usually called dynamic range, is the range from the discriminable or the resolvable minimum voltage difference to the recordable maximum voltage, and it depends on the bit length. When the length is 8 bits, its full scale, for example, from -1 to +1 volt, is divided into $2^8 = 256$. Thus, in this case, any differences smaller than $2/256$ volts in the amplitude are automatically ignored. If the bit length is 16 bits, the full scale from -1 to +1 volt is divided into $2^{16} = 65,536$ and much smaller differences can be discriminated. The dynamic range is from $7.8 \times 10^{-3} (= 2/256)$ to 2 V for 8 bits, whereas it is from $3.1 \times 10^{-5} (= 2/65,536)$ to 2 V for 16 bits.

When using amplitude data of the waveform in analysis, for example, to calculate the b-value using Gutenberg-Richter relation (Gutenberg and Richter 1942), a large dynamic range is essential. The unit “word” of a recording length is sometimes used, noting that one word corresponds to 8 bits (1 byte) where the bit length is 8 bits, whereas it corresponds to 16 bits (2 bytes) for a case of 16 bits.

(4) Continuous AE acquisition

A conventional transient recording system has a certain dead-time, where AE data are not recorded during this interval; this could result in loss of valuable information, especially in the case of a high level of AE activity. Continuous AE acquisition systems record without AE data loss, but the disadvantage of such systems is the huge dataset, requiring additional

software for processing. With the increase of installed memory, systems that can record all AE events continuously through an experiment have become commercially available. Since some researchers have already started to use this type of system, continuous monitoring (without trigger) may become increasingly popular in the near future.

The following examples show the capability of continuous AE acquisition. A continuous recorder was used to record 0.8 seconds at 10 MHz and 16 bits (Lei et al. 2003). A continuous AE recorder was used to store 268 seconds of continuous AE data on 16 channels at a sampling rate of 5 MHz and at 14-bit resolution (Thompson et al. 2005, 2006; Nasser et al. 2006). A more advanced continuous AE acquisition system, which can record continuously for hours at 10 MHz and 12 or 16 bits, was used within conventional triaxial and true-triaxial geophysical imaging cells (Benson et al. 2008; Nasser et al. 2014). In addition, there exists a combined system with the capability for conventional transient recording where there is a low AE activity and for recording AE continuously in the case of a high level of AE activity; this provides zero dead-time and avoids the loss of AE signals (Stanchits et al. 2011). A disadvantages of such a system is that it costs more than a conventional transient or a continuously recording system.

4. Analysis

AE data analysis could be classified into the four categories; (1) event rate analysis to evaluate the damage accumulation and fracture extension, (2) source location, (3) energy release and the Gutenberg-Richter relation, and (4) source mechanism. In this section, AE data analysis is explained in this order.

4.1 Event counting

The most basic type of AE data analysis involves counting events as a function of time. As shown in Figure 5, by comparing AE rates with change of stress, strain, or other measured quantity characterizing the response, valuable insight on the accumulation of damage and extension of fracture can be obtained. Various statistical modeling methods can be used to extract additional information, including the Kaiser effect (Lockner 1993; Lavrov 2003).

4.2 Source location

If waveforms of an AE event are recorded at a number of sensors, the source can be located, providing perhaps the most valuable information from AE. Different approaches can be taken to determine source locations of AE events, but a common approach is to use a non-linear least squares method to seek four unknowns, the source coordinates x , y , z , and an occurrence time t , knowing the P-wave arrival time at each sensor and the P-wave velocity

measured before the experiment under the assumption that it does not change through the experiment. A seminal contribution to the source location problem is the paper by Salamon and Weibols (1974). Other valuable references include Section 7.2 of Stein and Wysession (2003) and Section 5.7 of Shearer (2009). Source locations of AE events in laboratory experiments are reported in many papers (Lei et al. 1992; Zang et al. 1998, 2000; Fakhimi et al. 2002; Benson et al. 2008; Graham et al. 2010; Stanchits et al. 2011, 2014; Ishida et al. 2004, 2012; Yoshimitsu et al. 2014). In addition, the calculation of fractal dimension using spatial distributions of AE sources can be quite valuable in identifying localization (Lockner et al. 1991; Lei et al. 1992; Shah and Labuz 1995; Zang et al. 1998; Lei et al. 2003; Stanchits et al. 2011).

4.3 Energy release and the Gutenberg-Richter relation

A signal recorded at only one sensor should not be used to estimate energy released due to geometric attenuation of the signal. However, for a large number of sensors with sufficient coverage, an average root-mean-square (RMS) value from all the sensors will be representative of the AE energy. The RMS value is obtained by taking the actual voltage $g(t)$ at each point along the AE waveform and averaging the square of $g(t)$ over the time period T ; the square root of the average value gives the RMS value.

The Gutenberg-Richter relationship, originally proposed as a relation between magnitudes of earthquakes and their numbers, can also be applied to AE data. Mogi (1962a and 1962b) indicated through his laboratory experiments that the relation depends on the degree of heterogeneity of the material. Scholz (1968a) found in uniaxial and triaxial compression tests that the state of stress, rather than the heterogeneity of the material, plays the most important role in determining the relation. These findings have been applied in order to understand the phenomena of real earthquakes and the Gutenberg-Richter relationship is often used as an index value for fracturing in rock specimens (e.g. Lei et al. 1992, 2003; Lockner 1993; Zang et al. 1998; Stanchits et al. 2011).

4.4 Source mechanism

If the polarity of the initial P-wave motion at several sensors is identified, the source mechanism can be analyzed using a fault plane solution. The polarity of a waveform is defined as positive if the first motion is compressive or outward and negative if it is tensile or inward. Microcrack opening and volumetric expansion mechanisms cause positive first motions in all the directions around the source, whereas microcrack closing and pore collapse mechanisms cause all negative first motions. A pure sliding mechanism causes equal distributions of positive and negative polarities. The distribution of polarities for a mixed-mode mechanism (e.g. sliding with dilation) is more complex. Since the theory

applied to seismology can be directly applied to AE owing to the same physical mechanism of fracturing, the approach is described in several seismology texts, including Chapter 3 of Kasahara (1981), Section 4.2 of Stein and Wysession (2003), and Chapter 9 of Shearer (2009). The fault plane solutions of AE events in laboratory experiments are reported in Lei et al. (1992), Zang et al. (1998), and Benson et al. (2008).

With proper sensor calibration and simplifying assumptions (Davi et al. 2013; Kwiatek et al. 2014; Stierle et al. 2016), a detailed analysis of the source mechanism using the concept of the moment tensor can be performed. The AE source is characterized as a discontinuity in displacement, a microcrack, and represented by force dipoles that form the moment tensor. An inverse problem is solved for the six components of the moment tensor, which are then related to the physical quantities of microcrack displacement and orientation. In general, the directions of the displacement vector and the normal vector of the microcrack can be interchanged, but an angle 2α between the two vectors indicate opening when $\alpha = 0^\circ$, sliding when $\alpha = 45^\circ$, and anything in between is mixed-mode. The theory is reviewed in seismology texts e.g. Section 4.4 of Stein and Wysession (2003) and Chapter 9 of Shearer (2009), as well as in papers by Ohtsu and Ono (1986), Shah and Labuz (1995), and Manthei (2005). Applications of the moment tensor analysis to model AE events as microcracks are found in Kao et al. (2011), Davi et al. (2013), Kwiatek et al. (2014) and Stierle et al. (2016).

5. Reporting of Results

A report on AE laboratory monitoring should include the following:

- (1) Size, shape, and rock type of the specimen.
- (2) Size and frequency of the sensor and type (resonance or broadband).
- (3) Number of AE sensors used and sensor arrangement.
- (4) Block diagram of AE monitoring system or explanation of its outline.
- (5) Gain of pre- and main-amplifier of each channel.
- (6) Setting frequencies of high pass and low pass filter of each channel.
- (7) Threshold level of each channel for count rate and/or trigger for waveform recording.
- (8) If a triggering system is used, how to select AE sensors and how to use logical AND/OR for triggering. Dead time or continuous AE acquisition should be stated as well.
- (9) Sampling time, memory length (recording time period of each waveform), pre-trigger time and resolution of amplitude, if waveform is recorded.
- (10) Analysis of results, for example, AE count rate as a function of time, location of AE events, mechanisms of AE events including fault plane, moment tensor, or other solutions.
- (11) Other measured quantities related to the purpose of the experiment, for example, stress, strain, pressure and temperature, should be reported in comparison with the AE data.

References

- Benson PM, Vinciguerra S, Meredith PG, Young RP (2008) Laboratory simulation of volcano seismicity. *Science* 332(10): 249-252
- Boler FM, Spetzler HA, Getting IC (1984), Capacitance transducer with a point-like probe for receiving acoustic emissions, *Rev Sci Instrum* 55(8):1293-1297
- Chen LH, Labuz JF (2006) Indentation of rock by wedge-shaped tools. *Int J Rock Mech Min Sci* 43:1022-1033.
- Davi R, Vavryčuk V, Charalampidou E, Kwiatak G. (2013), Network sensor calibration for retrieving accurate moment tensors of acoustic emissions, *Int J Rock Mech Min Sci.*, 62: 59–67.
- Fakhimi A, Carvalho F, Ishida T, Labuz JF (2002) Simulation of failure around a circular opening in rock, *Int J Rock Mech Min Sci* 39: 507-515.
- Glaser, SD, Weiss GG, Johnson LR (1998). Body waves recorded inside an elastic half-space by an embedded, wideband velocity sensor. *J Acoust Soc Am.*, 104: 1404-1412.
- Goebel THW, Becker TR, Schorlemmer D, Stanchits S, Sammins C, Rybacki E, Dresen G (2012) Identifying fault heterogeneity through mapping spatial anomalies in acoustic emission statistics, *J Geophys Res* 117: B03310.
- Goodfellow S, Young R (2014) A laboratory acoustic emission experiment under in situ conditions, *Geophys Res Lett* 41: 3422-3430.
- Grosse CU, Ohtsu M (Eds.) (2008) *Acoustic Emission Testing* Springer-Verlag Berlin Heidelberg.
- Graham CC, Stanchits S, Main IG, Dresen G (2010) Source analysis of acoustic emission data: a comparison of polarity and moment tensor inversion methods, *Int J Rock Mech Min Sci* 47: 161–169.
- Gutenberg B, Richter CF (1942) Earthquake magnitude, intensity, energy and acceleration, *Bull Seismol Soc Am* 32: 163–191.
- Hardy Jr. HR (1994) Geotechnical field applications of AE/MS techniques at the Pennsylvania State University: a historical review, *NDT&E Int*, 27(4): 191-200.
- Hardy Jr. HR (2003) *Acoustic Emission/Microseismic Activity*, Vol. 1, Balkema.
- Heap MJ, Baud P, Meredith PG, Bell AF, Main IG (2009) Time-dependent brittle creep in Darley Dale sandstone. *J Geophys Res* 114: B07203.
- Ishida T, Chen Q, Mizuta Y, Roegiers J-C (2004) Influence of fluid viscosity on the hydraulic fracturing mechanism. *J Energy Resour Technol - Trans ASME* 126: 190-200.
- Ishida T, Aoyagi K, Niwa T, Chen Y, Murata S, Chen Q, Nakayama Y (2012) Acoustic emission monitoring of hydraulic fracturing laboratory experiment with supercritical and

- 443 liquid CO₂. *Geophys Res Lett* 39: L16309.
- 444 Kaiser J (1953) Erkenntnisse und Folgerungen aus der Messung von Geräuschen bei
445 Zugbeanspruchung von metallischen Werkstoffen. *Archiv für das Eisenhüttenwesen* 24:
446 43-45.
- 447 Kanagawa T, Hayashi M, Nakasa H (1976) Estimation of spatial components in rock samples
448 using the Kaiser effect of acoustic emission, CRIEPI (Central Research Institute of
449 Electric Power Industry) Report, E375004.
- 450 Kanagawa T, Nakasa H (1978) Method of estimating ground pressure, US Patent No. 4107981.
- 451 Kao C-S, Carvalho FCS, Labuz JF (2011) Micromechanisms of fracture from acoustic
452 emission. *Int J Rock Mech Min Sci* 48: 666-673.
- 453 Kasahara K (1981), *Earthquake mechanics*, Cambridge University Press, p. 248.
- 454 Kusunose K, Nishizawa O (1986) AE gap prior to local fracture of rock under uniaxial
455 compression. *J Phys Earth* 34(Supplement): S-45-S56.
- 456 Kwiatak G, Plenkers K, Dresen G, JAGUARS Research Group (2011) Source parameters of
457 picoseismicity recorded at Mponeng deep gold mine, South Africa: implications for
458 scaling relations, *Bull Seismol Soc Am* 101: 2592–2608.
- 459 Kwiatak G, Charalampidou E, Dresen G, Stanchits S. (2014) An improved method for seismic
460 moment tensor inversion of acoustic emissions through assessment of sensor coupling
461 and sensitivity to incidence angle, *Int J Rock Mech Min Sci*, 65, 153–161.
- 462 Lavrov A (2003) The Kaiser effect in rocks: Principles and stress estimation techniques, *Int J*
463 *Rock Mech Min Sci*, 40: 151-171.
- 464 Lei X, Nishizawa O, Kusunose K, Satoh T (1992) Fractal structure of the hypocenter
465 distributions and focal mechanism solutions of acoustic emission in two granites of
466 different grain sizes. *J. Phys. Earth* 40: 617-634.
- 467 Lei X, Kusunose K, Satoh T, Nishizawa O (2003) The hierarchical rupture process of a fault:
468 an experimental study. *Physics of the Earth and Planetary Interiors* 137:213-228.
- 469 Lockner DA, Byerlee JD, Kuksenko V., Ponomarev A, Sidorin A (1991) Quasi-static fault
470 growth and shear fracture energy in granite, *Nature* 350: 39-42.
- 471 Lockner DA (1993) Role of acoustic emission in the study of rock fracture, *Int J Rock Mech*
472 *Min Soc Geomech Abstr*, 30: 884-899.
- 473 Manthei G (2005) Characterization of acoustic emission sources in rock salt specimen under
474 triaxial compression. *Bull Seismol Soc Amer* 95(5): 1674-1700.
- 475 McLaskey G, Glaser S (2012) Acoustic emission sensor calibration for absolute source
476 measurements. *J Nondestruct Eval* 31: 157-168.
- 477 McLaskey G, Kilgore B, Lockner D, Beeler N (2014) Laboratory generated M-6
478 earthquakes. *Pure Appl Geophys* 171: 2601-2615.
- 479 Mogi K (1962a) Study of the elastic shocks caused by the fracture of heterogeneous

- 480 materials and its relation to earthquake phenomena, Bull. Earthquake Res. Inst., Tokyo
481 Univ. , 40: 125-173.
- 482 Mogi K (1962b). Magnitude-frequency relation for elastic shocks accompanying fracture of
483 various materials and some related to problems in earthquakes, Bull Earthquake Res
484 Inst, Tokyo Univ, 40: 831-853.
- 485 Mogi K (1968) Source locations of elastic shocks in the fracturing process in rocks (1). Bull
486 Earthquake Res Inst, Tokyo Univ, 46: 1103-1125.
- 487 Mogi K (2006) Experimental Rock Mechanics. Taylor & Francis.
- 488 Nakayama Y, Inoue A, Tanaka M, Ishida T, Kanagawa T (1993) A laboratory experiment for
489 development of acoustic methods to investigate condition changes induced by excavation
490 around a chamber, Proc. Third Int. Symp. on Rockburst and Seismicity in Mines,
491 Kingston, 383-386.
- 492 Nasser MHB, Mohanty B, Young RP (2006) Fracture toughness measurements and acoustic
493 emission activity in brittle rocks. Pure Appl Geophys 163: 917-945
- 494 Nasser MHB, Goodfellow SD, Lombos L, Young RP, (2014) 3-D transport and acoustic
495 properties of Fontainebleau sandstone during true-triaxial deformation experiments. Int
496 J Rock Mech Min Sci 69:1-18.
- 497 Nishizawa O, Onai K, Kusunose, K (1984) Hypocenter distribution and focal mechanism of
498 AE events during two stress stage creep in Yugawara andesite. Pure Appl Geophys 112:
499 36-52.
- 500 Obert L, Duvall WI (1945) Microseismic method of predicting rock failure in underground
501 mining "Part II, Laboratory experiments", RI 3803, USBM.
- 502 Ohtsu M, Ono K (1986) The generalized theory and source representations of acoustic
503 emission, J Acoust Emiss 5(4), 124-133.
- 504 Proctor T (1982) An improved piezoelectric acoustic emission transducer, J Acoust Soc Am,
505 71, 1163-1168.
- 506 Salamon MDG, Wiebols GA (1974), Digital location of seismic events by an underground
507 network of seismometers using the arrival times of compressional waves, Rock Mech.
508 1974; 6 (2): 141-166.
- 509 Scholz CH (1968a) The frequency-magnitude relation of microfracturing in rock and its
510 relation to earthquake, Bull Seismol Soc Am 58: 399-415.
- 511 Scholz CH (1968b) Microfracturing and the inelastic deformation of rock in compression. J
512 Geophys Res 73(4): 1417- 1432.
- 513 Scholz CH (1968c) Experimental study of the fracturing process in brittle rock. J Geophys
514 Res 73(4): 1447-1454.
- 515 Scholz CH (2002) The Mechanics of Earthquakes and Faulting (Second Edition). Cambridge
516 University Press.

- 517 Sellers EJ, Kataka MO, Linzer LM (2003), Source parameters of acoustic emission events
518 and scaling with mining. *J. Geophys. Res.*, 108(B9), 2418 – 2433.
- 519 Shah KR, Labuz JF (1995), Damage mechanisms in stressed rock from acoustic emission, *J.*
520 *Geophys. Res.*, 100(B8), 15527-15539.
- 521 Shearer PM (2009) *Introduction to Seismology (Second Edition)*. Cambridge University Press.
- 522 Spetzler H, Sobolev G, Koltsov A, Zang A, Getting IC (1991), Some properties of unstable
523 slip on rough surfaces, *Pure Appl. Geophys* 137: 95-112.
- 524 Stanchits S, Mayr S, Shapiro S, Dresen G (2011), Fracturing of porous rock induced by fluid
525 injection, *Tectonophysics*, 503(1-2): 129-145.
- 526 Stanchits S, Surdi A, Gathogo P, Edelman E and Suarez-Rivera R (2014), Onset of
527 hydraulic fracture initiation monitored by acoustic emission and volumetric deformation
528 measurements. *Rock Mech Rock Eng*, 47(5): 1521-1532.
- 529 Stein S, Wysession M (2003), *An Introduction to Seismology, Earthquakes, and Earth*
530 *Structure*. Blackwell Publishing.
- 531 Stierle E, Vavryčuk V, Kwiatak G, Charalampidou E, Bohnhoff M (2016), Seismic moment
532 tensors of acoustic emissions recorded during laboratory rock deformation experiments:
533 sensitivity to attenuation and anisotropy. *Geophys J Int*, 205, 38–50.
- 534 Terada M, Yanagidani T, Ehara S (1984) AE rate controlled compression test of rocks. In:
535 Hardy Jr. HR, Leighton FW (eds) *Proc Third Conf on Acoustic Emission/Microseismic*
536 *Activity in Geologic Structure and Materials*, University Park, Pennsylvania, USA, Trans
537 Tech Publication, 159-171.
- 538 Thompson BD, Young RP, Lockner DA (2005) Observations of premonitory acoustic
539 emission on slip nucleation during a stick slip experiment in smooth faulted Westerly
540 granite. *Geophys Res Lett*. 32:L10304.
- 541 Thompson BD, Young RP, Lockner DA (2006) Fracture in Westerly granite under AE
542 feedback and constant strain rate loading: Nucleation, quasi-static propagation, and the
543 transition to unstable fracture propagation, *Pure Appl. Geophys.*163: 995-1019.
- 544 Xiao Y, Feng X, Hudson JA, Chen B, Feng G, Liu, J (2016) ISRM suggested method for in
545 situ microseismic monitoring of the fractured process in rock masses, *Rock Mech Rock*
546 *Eng* 49: 843-869.
- 547 Yanagidani T, Ehara S, Nishizawa O, Kusunose K, Terada M (1985) Localization of
548 dilatancy in Ohshima granite under constant uniaxial stress. *J Geophys Res* 90(B8):
549 6840-6858.
- 550 Yoshimitsu N, Kawakata H, Takahashi N (2014) Magnitude -7 level earthquakes: A new lower
551 limit of self-similarity in seismic scaling relationship, *Geophys Res Lett* 41: 4495-4502. .
- 552 Zang A, Wagner FC, Dresen G (1996) Acoustic emission, microstructure, and damage model
553 of dry and wet sandstone stressed to failure. *J Geophys Res* 101(B8): 17507-17521.

- 554 Zang A, Wagner FC, Stanchits S, Dresen G, Andresen R, Haidekker MA (1998) Source
555 analysis of acoustic emissions in Aue granite cores under symmetric and asymmetric
556 compressive loads. *Geophys J Int* 135: 1113-1130.
- 557 Zang A, Wagner FC, Stanchits S, Janssen C, Dresen G (2000) Fracture process zone in granite.
558 *J Geophys Res* 105(B10): 23651-23661.
- 559 Zietlow WK, Labuz JF. (1998) Measurement of the intrinsic process zone in rock using
560 acoustic emission. *Int. J. Rock Mech. Min. Sci.* 35(3): 291-299.

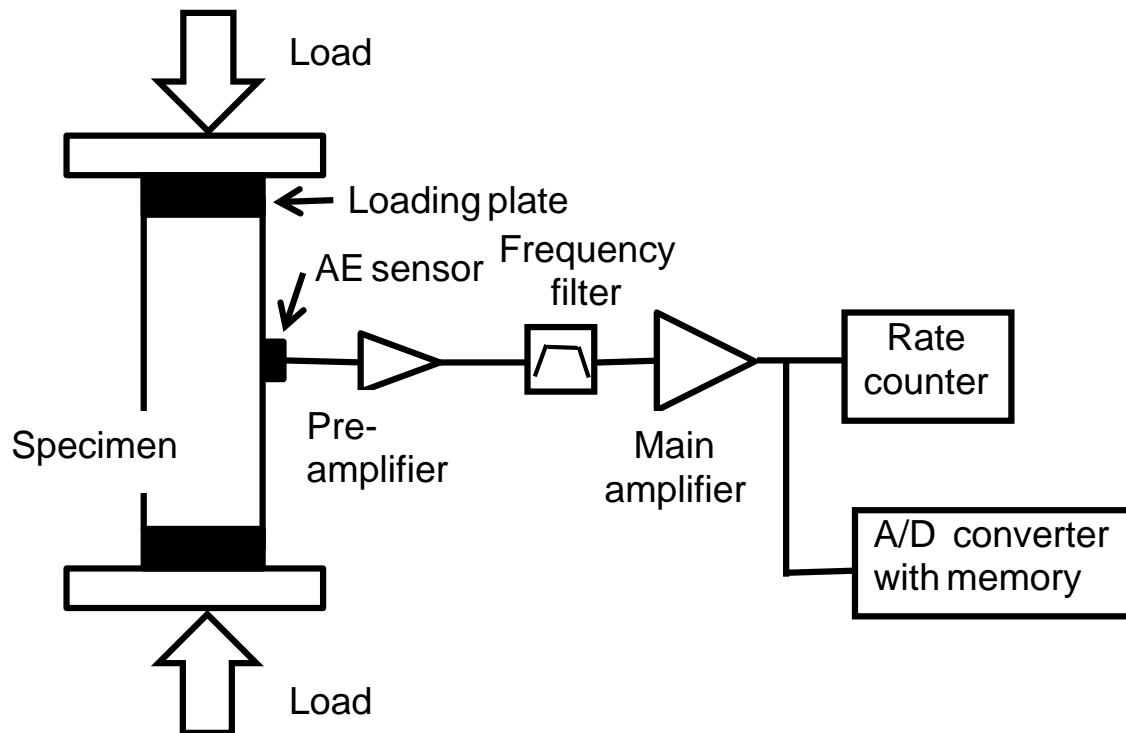
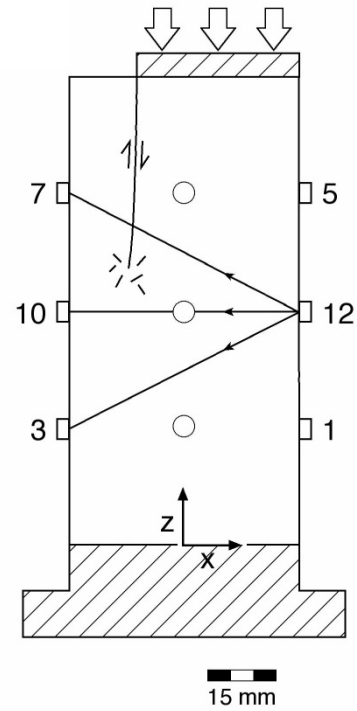


Figure 1. Typical AE monitoring system for a laboratory uniaxial compression test.



(a) Photograph

(b) Illustration

Figure 2. Example of the twelve sensor array for a core measuring 5 cm in diameter and 10 cm in length after Zang et al. (2000).



Figure 3. Typical AE sensor and pre-amplifier for a laboratory experiment. Coin is 24.26 mm in diameter (a quarter of US dollar) for scale.

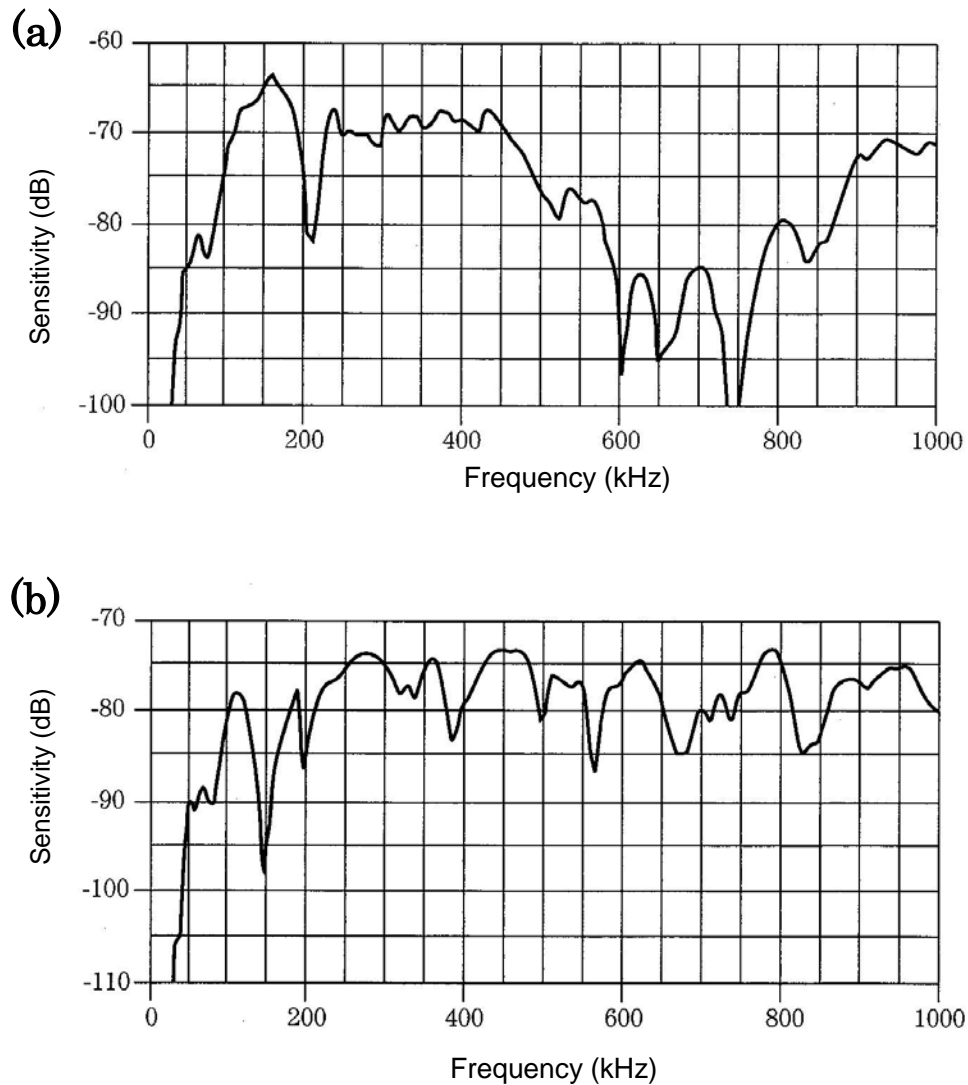


Figure 4. Examples of frequency response characteristics of AE sensors. (a) Resonance type sensor, PAC Type R15 with a resonance frequency 150 kHz. (b) Broadband type sensor, PAC Type UT1000. Both sensor models from Physical Acoustics Corporation, Princeton, NJ, USA.

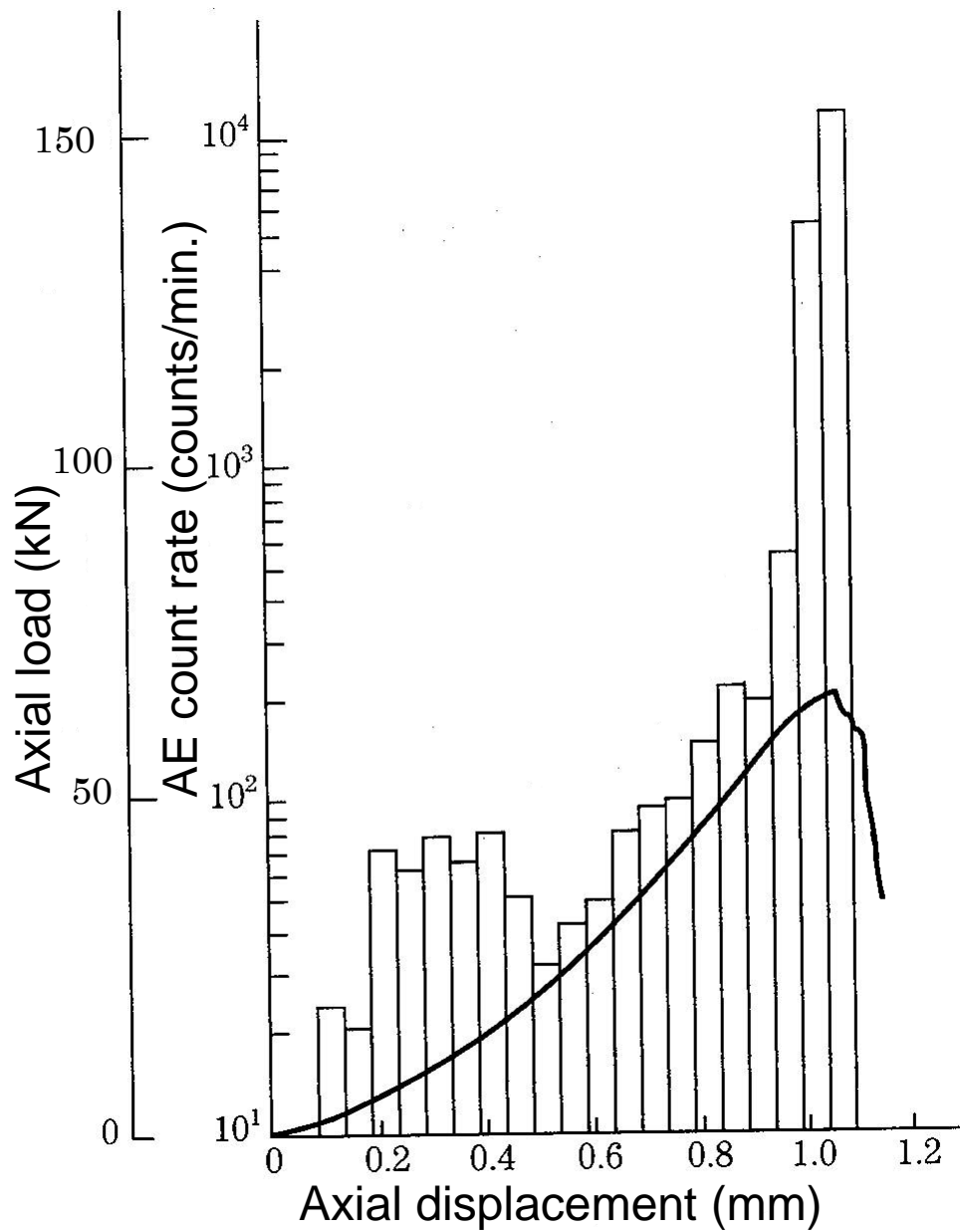


Figure 5. Typical AE count rate monitored in a uniaxial compression test under a constant axial displacement rate. The bar graph and the bold line indicate AE count rates and the load-displacement curve, respectively.

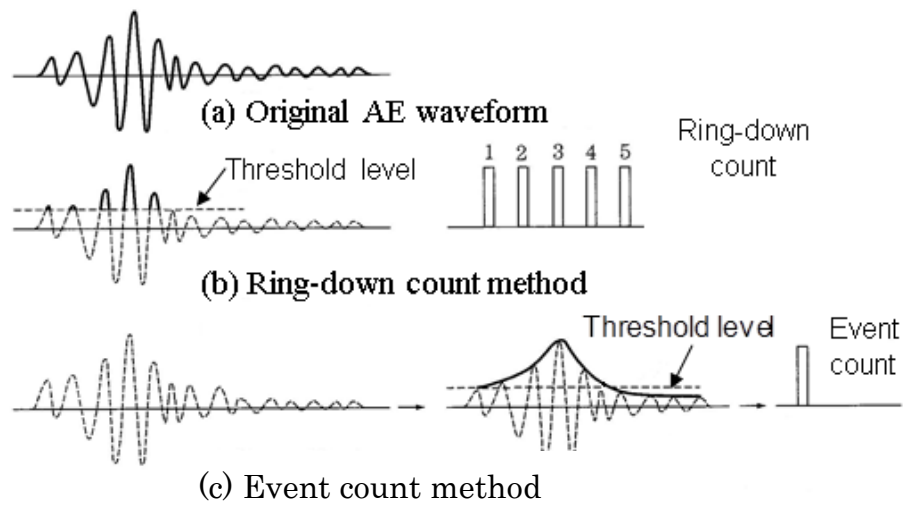


Figure 6. Two methods to count AE events. (a) The original AE waveform. (b) The ring-down count. (c) The event count.

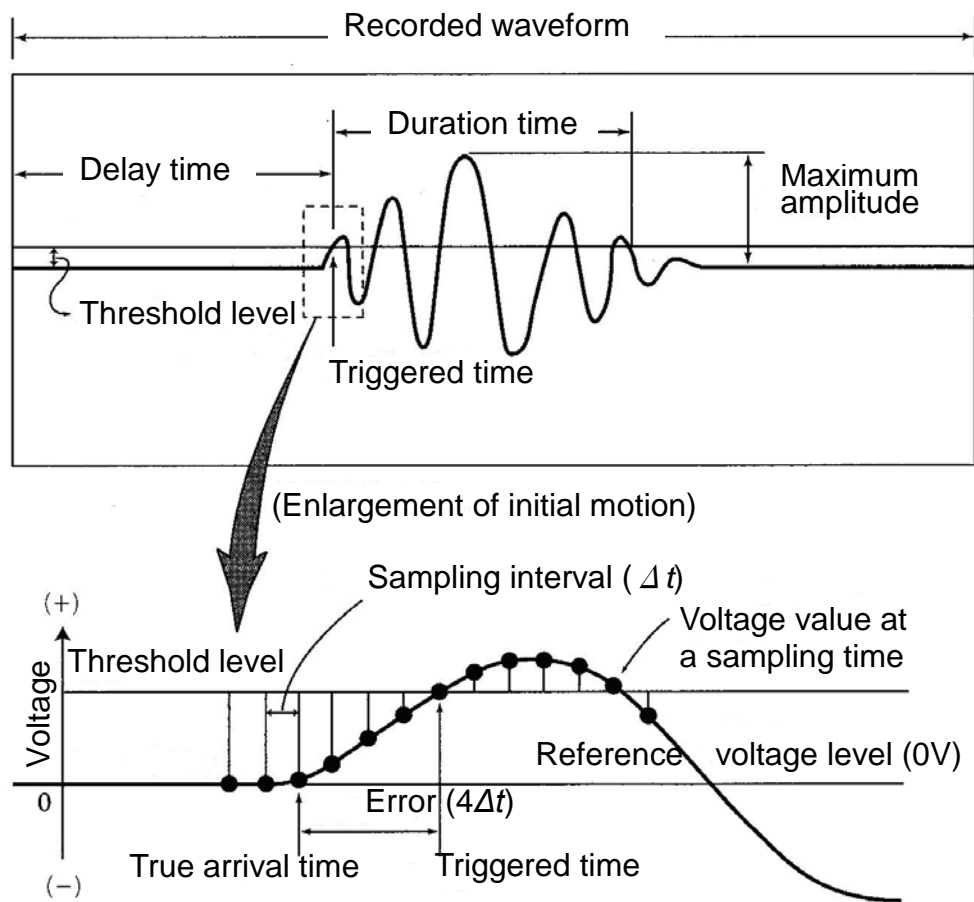


Figure 7. Example of recorded AE waveform and illustration of its Analog/Digital conversion.

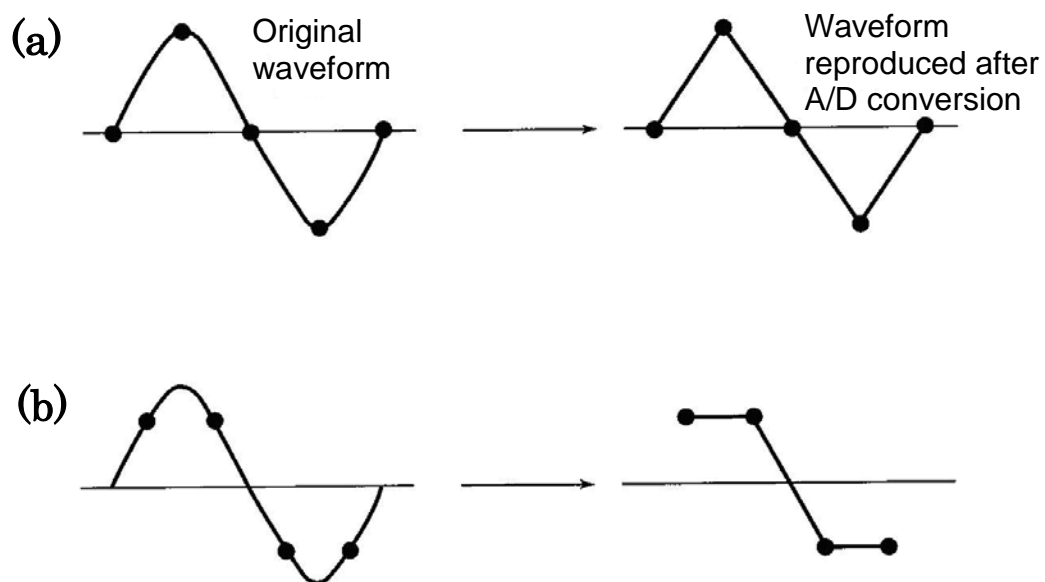


Figure 8. Relationship between an original waveform and a waveform reproduced after A/D conversion. (a) Ideal case where sampling points meet the maximum and the minimum points of the original waveform. (b) Actual case where the sampling points are displaced $1/8$ cycle along the time axis.